Available online at www.sciencedirect.com
SCIENCE DIRECT
Journal of Power Sources 158 (2006) 110–123
JOURNAL OF POWER SOURCES
www.elsevier.com/locate/jpowsour

Dynamic characteristics of spherical agglomerate for study of cathode catalyst layers in proton exchange membrane fuel cells (PEMFC)

R. Madhusudana Rao, R. Rengaswamy*

Department of Chemical Engineering, Clarkson University, Potsdam, NY 13699, USA

Received 14 August 2005; accepted 26 September 2005
Available online 28 November 2005

Abstract

There has been growing interest in the modeling of proton exchange membrane fuel cells (PEMFC) over the last two decades. While a variety of steady-state models have been proposed, literature is scarce in PEMFC dynamic models and transient studies. Typical dynamic models for PEM fuel cell are empirical current–voltage relationships. The internal transients associated with reactant and product species and other components are usually neglected. A detailed dynamic model for spherical agglomerate in PEM fuel cell is presented in this work. The dynamic model includes detailed mathematical equations for conservation of oxygen and hydrogen ions inside the agglomerate. The agglomerate dynamic model is simulated for typical operating conditions inside the PEMFC catalyst layer. Simulation studies show that the time scales in which the dynamics of agglomerate potential and concentration of dissolved oxygen respond differ by several orders of magnitude. Transient response of agglomerate current to step changes in surface boundary conditions are also presented. Reasons for the typical characteristics observed in the dynamic behavior of agglomerate current are also highlighted.

Keywords: PEMFC; Dynamic model; Fuel cell; Spherical agglomerates; Electrode analysis

1. Introduction

There has been considerable interest in the modeling of proton exchange membrane fuel cells (PEMFC), and a number of PEMFC models have been proposed in the literature over the last two decades. The seminal works in PEMFC modeling are published by Springer et al. [1] and Bernardi and Verbrugge [2,3]. Models proposed during the early years are typically one-dimensional and accounted for steady-state mass transport and electrochemical kinetics. Subsequently, both simplified and complex models in terms of dimensionality and physicochemical phenomena have been studied. These models have been used for a variety of purposes such as, prediction of the typical characteristic (current–potential) curves, parameter and operating conditions sensitivity analysis, structural and process optimization studies, and three-dimensional temperature, pressure and species concentration distributions in the case of fuel cell stacks. A common feature in most of these models was that the reaction or catalyst layer is not modeled in detail. The reaction layer is treated as an ultra-thin layer, thus neglecting the transport of reactant gases and products. Hence, the catalyst layer is treated as a source/sink boundary condition for transport equations in the gas diffusion layer. Contrary to this assumption, even if gas phase transport is neglected on the consideration of ultra-thin layer, the presence of ionomer in the reaction layer along with carbon and platinum makes transport within the pores of the ionomer important. Moreover, catalyst layer is the region where various limiting mechanisms can occur and thus, can have a strong influence on the overall performance of the cell.

It is widely accepted that gas-diffusion electrodes (GDEs) used in fuel cells are three-phase electrodes with a complex geometry consisting of conducting solid material for electron transfer, hydrophilic phase for ion transfer and open pores for gas transport. It is generally accepted that the major difficulty in fuel cell development lies with the kinetics of the oxygen electrode [4,5]. The hydrogen electrode kinetics is relatively much faster than that of the oxygen electrode. The structure and operation of hydrophobic electrodes have been studied for the first time under electron micrographs by Tantram and Tseung [6]. They established that the catalyst is present largely in the form of porous aggregates, which form a three-dimensional network throughout the electrode. Intermingled with this, there exists an interlocking

* Corresponding author. Tel.: +1 315 268 4423; fax: +1 315 268 6654.
E-mail address: raghu@clarkson.edu (R. Rengaswamy).

0378-7753/$ – see front matter © 2005 Published by Elsevier B.V.
doi:10.1016/j.jpowsour.2005.09.043

Nomenclature

a_a	effective area of catalyst site per unit volume of agglomerate (cm^2 Pt cm^{-3} agglomerate)
a_{H_2O}	activity of water in the ionomer
a_{pt}	effective area of Pt per unit weight of Pt (cm^2 Pt mg Pt^{-1})
C_{agg}	capacitance per unit volume of agglomerate (farad cm^{-3} agglomerate)
$c_{O_2,agg}$	concentration of dissolved oxygen inside the agglomerate (gmol cm^{-3})
$c_{O_2,film}$	concentration of dissolved oxygen inside the ionomer film (gmol cm^{-3})
$c^s_{O_2}$	saturation concentration of oxygen inside the ionomer pores (gmol cm^{-3})
$D_{O_2,agg}$	diffusivity of dissolved oxygen in ionomer pores inside the agglomerate (cm^2 s^{-1})
$D_{O_2,mem}$	diffusivity of dissolved oxygen in ionomer pores (cm^2 s^{-1})
F	Faraday constant (C gm equiv.$^{-1}$)
$H_{O_2,mem}$	Henry's constant for air–ionomer interface (atm cm^3 $gmol^{-1}$)
i_a	local current density (A cm^{-2} Pt)
i_o	exchange current density for oxygen reduction on Pt (A cm^{-2} Pt)
I_{agg}	instantaneous current from an agglomerate (A)
$\mathbf{j}_{agg}$	charge flux inside agglomerate (A cm^{-2})
$\mathbf{j}_{film}$	charge flux inside ionomer film (A cm^{-2})
m_{pt}	loading of catalyst in cathode catalyst layer (mg Pt cm^{-2})
n	no. of electrons taking part in oxygen reduction reaction
$p_{O_2,r}$	partial pressure of oxygen at the surface (atm)
$p_{H_2O,r}$	partial pressure of water vapor at the surface (atm)
$p^s_{H_2O}$	saturation pressure of water vapor (atm)
R	universal gas constant (J gmol K^{-1})
R_{orr}	rate of oxygen reduction reaction per unit volume of agglomerate (gmol cm^{-3} s)
r	radial distance inside an agglomerate from the center (cm)
r_{agg}	radius of agglomerate (cm)
T_{agg}	agglomerate temperature (K)
t	time (s)
t_{RL}	thickness of cathode catalyst layer (cm)
V_{agg}	potential of the solid phase inside the agglomerate measure against SHE (V)

Greek symbols

α	transfer coefficient
δ_{film}	thickness of ionomer film covering the agglomerate (cm)
ε_{agg}	fraction of volume occupied by ionomer inside agglomerate
ε_r	fraction of void volume inside cathode catalyst layer
η_r	local overpotential inside the agglomerate (V)
ϕ_{agg}	local potential inside agglomerate (V)
ϕ_{film}	local potential inside the ionomer film (V)
ϕ_r	potential at the ionomer surface (V)
κ_{agg}	conductivity of ionomer inside the agglomerate (mho m^{-1})
κ_{mem}	conductivity of ionomer film (mho m^{-1})
λ_{water}	water content inside the ionomer (mol H_2O mol^{-1} SO_3^-)

network of porous hydrophobic polytetrafluoroethylene (PTFE). In the cell, the hydrophilic catalyst network becomes flooded with the electrolyte while the hydrophobic PTFE allows for the gas to diffuse through it. They had shown that the performance of electrodes is dependent on the microstructure of porous catalyst aggregates. However, it is not clear whether any specific geometry was suggested for the catalyst aggregates.

As GDEs are difficult to characterize, one of the first assumptions that was made to model them was the concept of "flooded agglomerates", introduced by Giner and Hunter [7]. They have considered cyclindrical geometry for the agglomerates. Results were presented for alkaline oxygen electrode. The potential drop was assumed to change only in the axial direction and diffusion of the dissolved gases was assumed to be in the radial direction of the agglomerates. The effect of the cylindrical agglomerate radius on the current generated and its distribution were studied. Porous GDEs with the same assumptions have been extended to model the phosphoric acid fuel cells (PAFC) cathode and anode in detail [8,5]. Various transport and kinetic processes which take place in the porous electrodes were taken into account. The model was used in the simulation mode for predictive analysis and for electrode development process.

One of the drawbacks with the above-proposed flooded-agglomerate model is that it does not consider any tortuosity for the gas phase transport as the agglomerates are assumed to completely extend from the gas side to the electrolyte side. The cylindrical flooded-agglomerate model was modified by Celiker et al. [9] considering spherical geometry. They have investigated their model predictions by considering the cathodic reduction of oxygen in alkaline medium. Subsequently, many studies conducted by various researchers with the spherical flooded-agglomerate model were presented for alkaline fuel cells (AFC) [10,11] and PAFC [11–13].

Even in the case of PEM fuel cells, researchers have studied the effect of various phenomena in the catalyst layer based on flooded-agglomerate model [11,14–18]. Perry et al. [11] have developed a model for gas diffusion electrode that can be used as diagnostic tool for designing of fuel cells. The model is one-dimensional model for mass transport in the zone where Tafel kinetics is valid. The models presented were generally valid for any GDE with either liquid electrolyte (AFC and PAFC) or ion-exchange membrane (PEMFC). The model was used to study the effects of mass-transport limitations on the polarization characteristics of oxygen reduction reaction in the cathode.

Using negligible mass transfer resistance in the gas phase the model develops a function for evaluating the Thiele modulus for the catalyst-binder agglomerates. These relations along with ion transport equations are combined to develop a single variable second-order differential equation. Based on it, asymptotic solutions were developed at different limiting conditions. The model also predicts different Tafel slopes for distinct regions. The authors have also shown how the results may be used as a diagnostic tool for analyzing fuel cell cathode data. Siegel et al. [14] have proposed a steady-state two-dimensional PEMFC model based on agglomerate geometry for the catalyst layer. The agglomerates are characterized by mean diameter and a characteristic length. Based on the model results, it has been highlighted that the fuel cell performance is highly dependent on catalyst structure. Recently, a thin-film agglomerate model with cylindrical geometry was proposed for the cathode of a PEM fuel cell [15]. The model described was a two-phase, one-dimensional steady state, isothermal model for a PEMFC cathode. The authors presented simulation results confirming water-flooding situation in catalyst layers. Since the agglomerates are considered to be cylindrical and extend from gas diffusion layer to membrane, the model assumes that gas phase transport inside catalyst layer is straight. Wang et al. [18] have investigated transport and reaction kinetics in spherical agglomerates of cathode catalyst layer. They have considered two types of spherical agglomerates: the first one consisting of a mixture of carbon/catalyst particles and perfluorosulfonated ionomer (PFSI) and the other type consisting of carbon/catalyst particles and water-filled pores. The model has been used to study current conversion, reactant and current distribution and catalyst utilization. The significance of these results for optimization of catalyst layers have also been highlighted.

One of the probable reasons for neglecting reaction layer in PEMFC models published in the beginning could be lack of instrumentation to characterize its morphology accurately. With the availability of advanced microscopy instruments like scanning electron microscopy (SEM) and transmission electron microscopy (TEM), researchers have been able to study the morphology of complex nanostructures such as, PEM fuel cell electrodes. Middleman [19] has studied the structure of membrane-electrode-assembly (MEA) using high-resolution scanning electron microscopy (HR-SEM). In his investigation he has shown that the catalyst layer consists of a random distribution of pores and particles, see Fig. 1. It was also shown, using higher magnification, that the particles are agglomerates of much smaller particles coated with a film of Nafion. From the images in the figure it can be clearly seen that the agglomerates are spherical in shape. Lee et al. [20] and Liu et al. [21] have also published their investigations of PEM fuel cell electrodes using SEM/TEM that corroborate Middleman's work. Therefore, spherical agglomerates are not an abstract conceptualization, but a realistic representation of cathode catalyst layers in PEM fuel cells for modeling purposes.

In this work, the transient characteristics of various transport and electrochemical phenomena are studied in spherical agglomerates using its dynamic model. For PEM fuel cells, flooded-agglomerate is a uniform mixture of Pt supported carbon particles and ionomer. In addition, to the study the effect of ionomer layer, we also consider a thin film of ionomer covering the agglomerate. We propose a detailed dynamic study of the spherical agglomerate for the following reasons:

- This is the first time in PEM fuel cell literature that an agglomerate dynamic model is being studied. The dynamic model has been used to study the dynamics of both dissolved concentration of oxygen ($c_{O_2,agg}$ and $c_{O_2,film}$) and hydrogen ions (ϕ_{agg} and ϕ_{film}).
- An agglomerate is a microcosm of the reaction layer. There are species transport and electrochemical phenomena taking place inside the agglomerate. Transport is in the form of diffusion of dissolved oxygen and hydrogen ions through the water-filled ionomer pores, and oxygen reduction reaction at the active catalyst sites producing water. Hence, it is expected that the steady-state and dynamic characteristics of an agglomerate are similar to that of the fuel cell characteristics.
- The dynamics of a complete PEM fuel are not very well understood. Moreover, the final dynamic model for the electrode is likely to be complicated. In view of this, we intend to study the simplifications that are possible for the complete reaction layer level model using the proposed dynamic spherical agglomerate model.

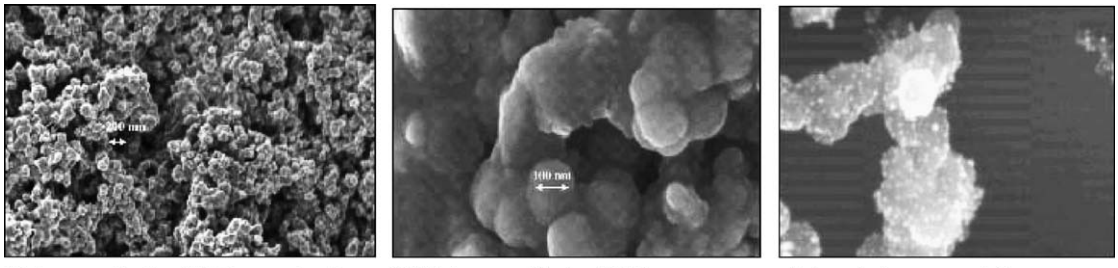

Fig. 1. Scanning electron microscope (SEM) images of PEM fuel cell electrode [19].

- We will demonstrate very interesting dynamic behavior such as phenomenon occurring at different time scales and delays at the agglomerate level. The insights developed through this model will significantly enhance the analysis of the full dynamic electrode model.
- The proposed dynamic spherical agglomerate model is the back-bone for an integrated reaction layer model for the cathode and anode.

The dynamic model for the agglomerate describes the conservation of dissolved oxygen and hydrogen ions, which is described in detail in the subsequent section. In the subsequent sections of the paper, hydrogen ions and charge are used synonymously. Typical steady-state agglomerate *i–v* characteristic curves are studied. Simulation results to show the effect of boundary conditions and model parameters on the *i–v* curves are also presented. The dynamic model is simulated to show the effect of step changes in the surface boundary conditions on the agglomerate current. Characteristic behavior observed through simulations in the agglomerate current are also explained.

2. Spherical agglomerate dynamic model

A schematic of the spherical agglomerate considered in this work is illustrated in Fig. 2. The agglomerate consists of a thin film of ionomer covering a uniform mixture of carbon supported Pt nanoparticles and ionomer in between the carbon agglomerates. At the surface, oxygen present in the gas dissolves into the water present inside the pores of the ionomer. At the surface it is assumed that there exists an equilibrium between the partial pressure of oxygen in the gas phase and the dissolved concentration in the ionomer phase. The dissolved oxygen diffuses through the ionomer pores towards the center of the agglomerate. No reactions are considered in the thin film of ionomer. Within the uniform mixture region, dissolved oxygen is assumed to diffuse towards the center simultaneously undergoing the following chemical reaction at the active catalyst sites:

$$O_2 + 4H^+ + 4e^- \rightarrow 2H_2O \tag{1}$$

The hydrogen ions produced in the anode catalyst layer travel across the membrane layer and reach active catalyst sites inside the agglomerate through a network of micropores in the ionomer. The following assumptions are considered for setting up the dynamic model equations:

- axisymmetric conditions are assumed for concentration and charge distribution inside the agglomerate,
- pressure and temperature conditions are uniform throughout the agglomerate,
- the contribution due to convection for species flux is negligible,
- charge accumulation takes place only near the surface of Pt,
- Butler–Volmer kinetics are considered for the oxygen reduction reaction,
- physical properties of the ionomer are considered same as that of the membrane,

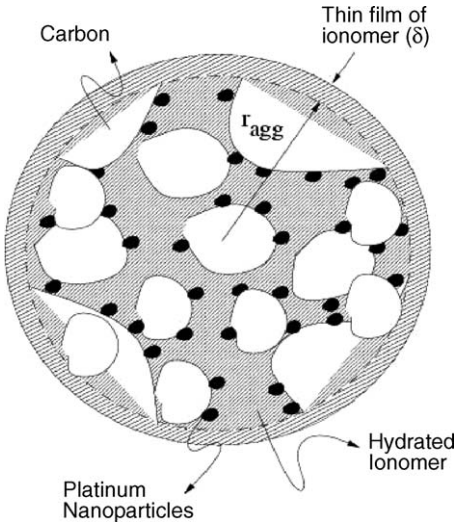

Fig. 2. Spherical flooded-agglomerate with ionomer film.

- potential of the solid phase (C + Pt) is assumed to be uniform throughout the agglomerate.

The conservation equations for oxygen and hydrogen ions are written separately for the ionomer film and the agglomerate.

2.1. Conservation equations inside ionomer film

Since no reactions are considered inside the ionomer film, the dynamic conservation equation for oxygen inside the film can be written as

$$\frac{\partial}{\partial t}(c_{O_2,\text{film}}) = \frac{D_{O_2,\text{mem}}}{r^2}\frac{\partial}{\partial r}\left(r^2\frac{\partial c_{O_2,\text{film}}}{\partial r}\right) \tag{2}$$

where r is the radial distance from the center of the agglomerate and $D_{O_2,\text{mem}}$ is the diffusivity of dissolved oxygen inside the ionomer pores. With the above assumptions, the dynamic conservation equation for charge flux would reduce to

$$-\nabla \cdot \mathbf{j}_{\text{film}} = 0 \tag{3}$$

where the charge flux, $\mathbf{j}_{\text{film}}$, is related by ohm's law to the potential inside film (ϕ_{film}) as

$$\mathbf{j}_{\text{film}} = -\kappa_{\text{mem}}\nabla(\phi_{\text{film}}) \tag{4}$$

Therefore, Eq. (3) can be written as

$$\frac{\kappa_{\text{mem}}}{r^2}\frac{\partial}{\partial r}\left(r^2\frac{\partial \phi_{\text{film}}}{\partial r}\right) = 0 \tag{5}$$

The membrane conductivity, κ_{mem}, is a function of water content inside the ionomer pores, λ_{water}, which in turn is a function of the activity of water. The activity is water is given by

$$a_{H_2O} = \frac{p_{H_2O,r}}{p^s_{H_2O}} \tag{6}$$

where the saturation pressure of water vapor, $p^s_{H_2O}$ is dependent on the local temperature conditions and is calculated by the

following equation:

$$p^{s}_{H_2O} = \frac{1.02}{1000}(T_{agg})^{-4.9283}10^{(23.5518-(2937.8/T_{agg}))} \quad (7)$$

The ionomer water content is calculated from [1]:

$$\lambda_{water} = 0.043 + 17.81a_{H_2O} - 39.85a^2_{H_2O} + 36.0a^3_{H_2O},$$
$$\text{for } 0 < a_{H_2O} \leq 1$$
$$= 14.0 + 1.4(a_{H_2O} - 1),$$
$$\text{for } 1 \leq a_{H_2O} \leq 3 \quad (8)$$

The membrane conductivity is calculated by the following equation [1]:

$$\kappa_{mem} = (0.005139\lambda_{water} - 0.00326) \times \exp\left[1268.0\left(\frac{1}{303.0} - \frac{1}{T_{agg}}\right)\right] \quad (9)$$

2.2. Conservation equations inside the agglomerate region

The dynamic conservation equation for oxygen inside the agglomerate can be written as

$$\frac{\partial}{\partial t}(c_{O_2,agg}) = \frac{D_{O_2,agg}}{r^2}\frac{\partial}{\partial r}\left(r^2\frac{\partial c_{O_2,agg}}{\partial r}\right) + R_{orr} \quad (10)$$

where $D_{O_2,agg}$ is the diffusion coefficient of dissolved oxygen in the ionomer pores inside the agglomerate. It is related to $D_{O_2,mem}$ and fraction of ionomer volume inside the agglomerate (ε_{agg}) as

$$D_{O_2,agg} = \varepsilon^{3/2}_{agg}D_{O_2,mem} \quad (11)$$

The oxygen reduction reaction (R_{orr}) is given by Butler–Volmer kinetics as

$$R_{orr} = -\frac{a_a i_a}{nF} \quad (12a)$$

$$= -\frac{a_a}{n_e F}i_o\left\{\frac{c_{O_2,agg}}{c^s_{O_2}}\exp\left(-\frac{\alpha n_e \eta_r F}{RT_{agg}}\right) - \exp\left(\frac{(1-\alpha)n_e\eta_r F}{RT_{agg}}\right)\right\} \quad (12b)$$

The local overpotential (η_r) appearing in the Butler–Volmer kinetics is the defined by the following equation

$$\eta_r = \Delta\phi(s, agg) - \Delta\phi_e(s, agg) \quad (13a)$$
$$= \{\phi_s - \phi_{agg}\} - \{\phi_{e,s} - \phi_{e,agg}\} \quad (13b)$$

where ϕ_s is the potential of the solid phase and ϕ_{agg} is ionomer potential adjacent to carbon and platinum. The subscript e denotes equilibrium conditions. If oxygen electrode is treated as the reference electrode, then solid phase potential $\phi_s = 0$ and $\Delta\phi_e(s, agg) = 0$. In such a case, the local overpotential appearing in the Butler–Volmer equation (η_r) is numerically equal to the local ionomer potential (ϕ_{agg}). The active surface area of platinum per unit volume of agglomerate (a_a) is related to platinum loading (m_{pt}), effective area of platinum (a_{pt}), catalyst layer thickness (t_{RL}), and void fraction inside the catalyst layer (ε_r) by the following equation

$$a_a = \frac{m_{pt}a_{pt}}{(1-\varepsilon_r)t_{RL}} \quad (14)$$

The saturation concentration of dissolved oxygen, $c^s_{O_2}$, is given by Henry's law applied at the surface of the ionomer film:

$$c^s_{O_2} = \left(\frac{1}{H_{O_2,mem}}\right)p_{O_2,r} \quad (15)$$

Writing the dynamic conservation equation for charge gives

$$\frac{\partial}{\partial t}(C_{agg}\eta_r) = -\nabla\cdot\mathbf{j}_{agg} + n_e F R_{orr} \quad (16)$$

where η_r is the local overpotential inside the agglomerate at a radial distance r from the center and C_{agg} is capacitance per unit volume of agglomerate. For writing the above conservation equation, both capacitative and faradaic currents are taken into consideration. The left-hand side of the equation represents accumulation of hydrogen ions in the double layer near the platinum surface. The faradaic current is represented by the reaction term (R_{orr}). The charge flux inside the agglomerate, $\mathbf{j}_{agg}$, is given by

$$\mathbf{j}_{agg} = -\kappa_{agg}\nabla(\phi_{agg}) \quad (17)$$

The conductivity of hydrated ionomer inside the agglomerate, κ_{agg}, is related to membrane conductivity as

$$\kappa_{agg} = \varepsilon^{3/2}_{agg}\kappa_{mem} \quad (18)$$

Eq. (16) can be written as

$$\frac{\partial}{\partial t}(C_{agg}\eta_r) = \frac{\kappa_{agg}}{r^2}\frac{\partial}{\partial r}\left(r^2\frac{\partial\phi_{agg}}{\partial r}\right) + n_e F R_{orr} \quad (19)$$

Eqs. (2), (5), (10) and (19) are solved for the concentration of dissolved O_2 and potential inside the agglomerate and ionomer film. The initial and boundary conditions are given in Table 1. Henceforth, the potential at the surface of ionomer film (ϕ_r) will be called as surface potential in the paper.

The agglomerate current can be calculated by several methods. For the steady-state model, the agglomerate current was calculated by the following equations, which are all equivalent

$$I_{agg} = -n_e F 4\pi r^2_{agg} D_{O_2,film}\frac{\partial c_{O_2,film}}{\partial r}|_{r=r_{agg}} \quad (20a)$$
$$= -n_e F 4\pi r^2_{agg} D_{O_2,agg}\frac{\partial c_{O_2,agg}}{\partial r}|_{r=r_{agg}} \quad (20b)$$
$$= -4\pi r^2_{agg}\kappa_{mem}\frac{\partial\phi_{film}}{\partial r}|_{r=r_{agg}} \quad (20c)$$
$$= -4\pi r^2_{agg}\kappa_{agg}\frac{\partial\phi_{agg}}{\partial r}|_{r=r_{agg}} \quad (20d)$$
$$= \int_0^{r_{agg}} 4\pi r^2(n_e F R_{orr})\,dr \quad (20e)$$

In the case of dynamic model, for determining the instantaneous current generated inside an agglomerate, local reaction rate along with charge accumulation term is integrated over the

Table 1
Initial and boundary conditions for spherical agglomerate in Fig. 2

Number	Initial and boundary conditions	Comments
t = 0		
IC1	$c_{O_2,film} \forall r$	Obtained from steady-state solution
IC2	$c_{O_2,agg} \forall r$	Obtained from steady-state solution
IC3	$\phi_{film} \forall r$	Obtained from steady-state solution
IC4	$\phi_{agg} \forall r$	Obtained from steady-state solution
r = $r_{agg} + \delta_{film}$		
BC1	$c_{O_2,film} = \left(\frac{1}{H_{O_2,mem}}\right) p_{O_2,r} \forall t$	Equilibrium at interface
BC2	$\phi_{film} = \phi_r \forall t$	Surface boundary condition
r = r_{agg}		
BC3	$c_{O_2,agg} = \varepsilon_{agg} c_{O_2,film} \forall t$	Continuity
BC4	$-D_{O_2,mem} \frac{\partial c_{O_2,film}}{\partial r} = -D_{O_2,agg} \frac{\partial c_{O_2,agg}}{\partial r} \forall t$	Species flux condition
BC5	$\phi_{agg} = \phi_{film} \forall t$	Continuity
BC6	$-\kappa_{mem} \frac{\partial \phi_{film}}{\partial r} = -\kappa_{agg} \frac{\partial \phi_{agg}}{\partial r} \forall t$	Charge flux condition
r = 0		
BC7	$\frac{\partial c_{O_2,agg}}{\partial r} = 0 \quad \forall t$	
BC8	$\frac{\partial \phi_{agg}}{\partial r} = 0 \quad \forall t$	

entire agglomerate volume and expressed in current equivalent and is given by the following equation:

$$I_{agg} = \int_0^{r_{agg}} 4\pi r^2 \left\{ -n_e F R_{orr} + \frac{\partial}{\partial t}(\eta_r C_{agg}) \right\} dr \tag{21}$$

3. Results and discussion

The model equations were set up Maple (version 9) and were solved using fsolve (for steady-state case) and ode15s (for dynamic case), which are available in MATLAB. For generating initial guess for the dynamic model, steady-state model corresponding to the dynamic model equations enumerated above are solved first.

3.1. Steady-state model simulation

The steady-state model is set up such that, surface potential (ϕ_r), partial pressures of oxygen ($p_{O_2,r}$) and water vapor ($p_{H_2O,r}$) at the surface of ionomer film and temperature of the agglomerate (T_{agg}) are taken as inputs. The dissolved concentration of oxygen ($c_{O_2,agg}$ and $c_{O_2,film}$), potential variation inside ionomer film and agglomerate (ϕ_{agg} and ϕ_{film}), and the current generated from the agglomerate (I_{agg}) are the output variables. Simulation studies are carried out using the steady-state model to study the *i–v* characteristic curve and the influence of boundary conditions and other parameters on the curve. The base case model parameters and their range for parameter sensitivity studies are listed in Table 2.

For discretizing the PDEs, a certain number of points are chosen along the radius of the agglomerate and finite difference techniques are applied. Before describing the model results, the sensitivity of the results to the number of points chosen is briefly discussed here. Preliminary steady-state simulation results showed that oxygen concentration profiles inside ionomer film and agglomerate were sensitive to the number of points chosen along the radius. As a result, the *i–v* curves also showed variation. Hence, simulations were performed by increasing the number of points till the results showed no variation. In addition, it was also observed that the number of points inside the agglomerate (N_{agg}) and ionomer film (N_{film}) have to be same. In all the results presented below, $N_{agg} = N_{film} = 500$. For the sake of clarity, even though 500 points are chosen along the radius in the agglomerate and ionomer film, only fewer number of points are shown in the plots. Figs. 3 and 4 illustrate the concentration profiles of dissolved oxygen inside the agglomerate and ionomer film, respectively, at different surface potentials. The plots show that as surface potential is decreased, gradients of the concentration profiles become steeper. This is due to an increase in reaction rate as the surface potential is decreased. When the surface potential is decreased beyond −0.20 V, it was observed that the concentration profiles have more steeper gradients. These results show that even though the thickness of ionomer film is very small (in the range of 0.01–0.10 μm) considerable concentration gradients exist, contrary to the assumptions made by other researchers [15,18].

Since an agglomerate is a microcosm of the reaction layer, it will be expected that the characteristic curve of an agglomerate is similar to that of the fuel cell characteristic curve. Fig. 5 illustrates the *i–v* characteristic curve for the spherical agglomerate, which conforms to the typical fuel cell characteristic plot. The curve is marked by the legend "With variation in potential" in Fig. 5. The other *i–v* curve in the figure corresponds to the case when potential is considered constant inside the ionomer film and agglomerate, an assumption considered by Wang et al. [18] for PFSI filled spherical agglomerate. With this assumption, only the steady-state oxygen conservation equation needs to be solved. In fact, an analytical solution can be obtained for the

Table 2
Model inputs and parameters

Parameter	Base case value	Range for parameter studies	Units	Reference
Inputs				
$p_{O_2,r}$	0.50	0.05–0.50	atm	
$p_{H_2O,r}$	0.24	0.10–0.60	atm	
ϕ_r	0.0 to −0.40		V	
T_{agg}	353.15		K	
Model parameters				
a_{pt}	1000	–	cm^2 Pt mg^{-1} Pt	[15]
C_{rxn}	20.0×10^{-6}		Farad cm^{-2} Pt	[22,23]
$D_{O_2,mem}$	$3.1 \times 10^{-3} \exp\left(-\frac{2768}{T_{agg}}\right)$		$cm^2\ s^{-1}$	[24,2]
F	96485.3		C g equiv.$^{-1}$	
$H_{O_2,mem}$	$1.33 \times 10^{6} \exp\left(-\frac{666.0}{T_{agg}}\right)$		atm cm^3 $gmol^{-1}$	[3]
i_o	6.0×10^{-8}		A cm^{-2}	[14]
m_{pt}	0.40	0.10–1.0	mg Pt cm^{-2}	[15]
n_e	4			
R	8.314		J $gmol\ K^{-1}$	
r_{agg}	1.0×10^{-4}	1.0×10^{-5} to 1.0×10^{-4}	cm	
T_{agg}	353.15		K	
t_{RL}	30		μm	
α	0.50			
δ_{film}	1.0×10^{-5}	5.0×10^{-6} to 5.0×10^{-5}	cm	
ε_{agg}	0.40	0.10–0.50		[3]
ϵ_r	0.40			[3]

agglomerate current (I_{agg}), which was obtained using Maple. A comparison of the two *i–v* curves clearly shows the difference and the significance of considering variation in potential inside the ionomer film and agglomerate instead of assuming it to be constant.

Another important feature to be noted from the plot is that the current from the agglomerate stagnates beyond a certain surface potential (−0.35 V). This is due to the fact that at these potentials, the dissolved oxygen is completely consumed within a short radial distance from the surface inside the agglomerate region. In fact, it can be observed from Fig. 3 that beyond a certain potential, oxygen is completely utilised at the surface of the agglomerate itself and there is not enough supply of oxygen to reach the center of the agglomerate. Hence, a large part of the agglomerate does not produce any current due to lack of oxygen.

Parametric studies were carried out on the steady-state model of the agglomerate to study the effect of boundary conditions and model parameters on the characteristic curve. For parametric studies using the model, a range of values are considered for a particular parameter and base case values are taken for the other parameters. The steady state model was simulated for different values of surface boundary conditions ($p_{O_2,r}$, and $p_{H_2O,r}$)

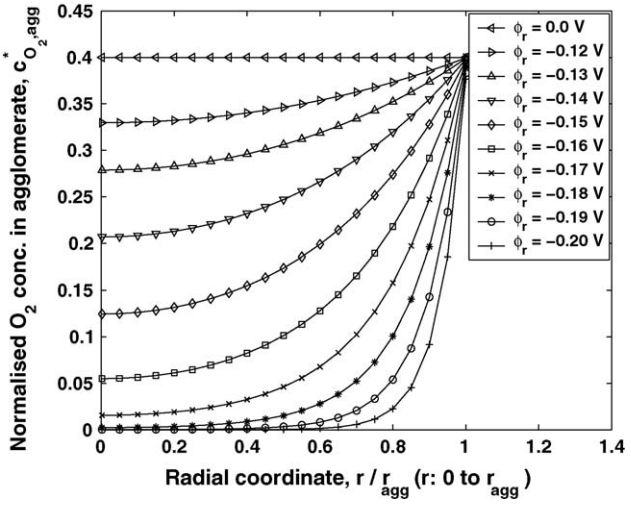

Fig. 3. Normalised concentration of O_2 as a function of radial distance inside agglomerate for different surface potentials (ϕ_r).

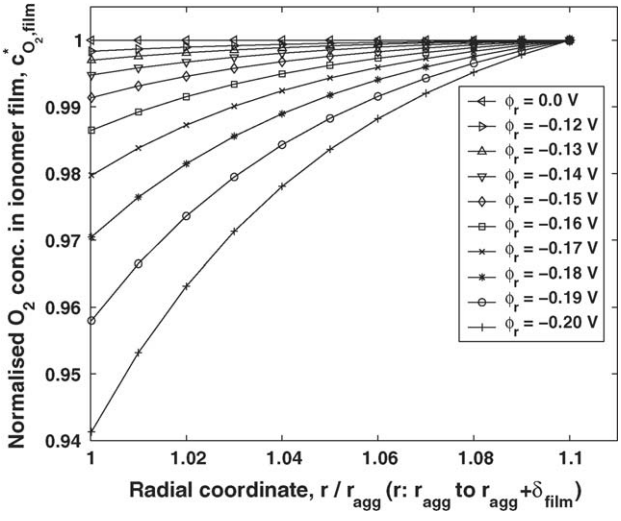

Fig. 4. Normalised concentration of O_2 as a function of radial distance inside ionomer film for different surface potentials (ϕ_r).

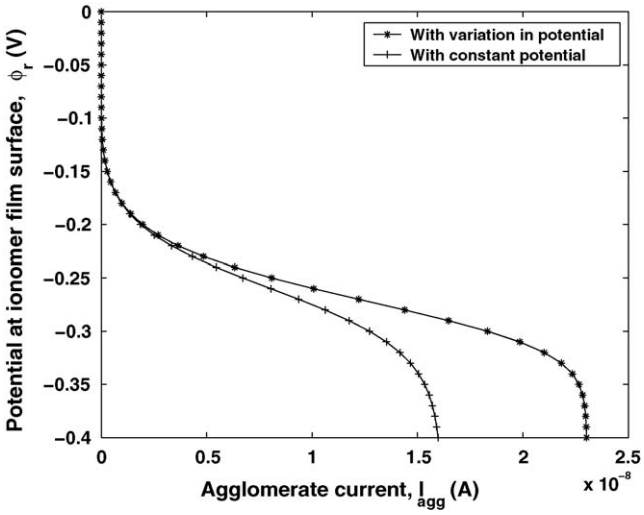

Fig. 5. *I–V* characteristic curve for agglomerate shown in Fig. 2.

and model parameters (m_{pt}, ε_{agg}, r_{agg} and δ_{film}). Fig. 6(a) shows the characteristic curves for different values of partial pressure of oxygen at the ionomer surface. With an increase in partial pressure of oxygen in the gas phase, the equilibrium concentration of dissolved oxygen just inside the ionomer increases. Hence, as it would be expected, larger amounts of current are generated from the agglomerate and this trend can be clearly seen in the figure. Contrary to the above result and expectations, increasing the partial pressure of water vapor at the surface does not have any significant effect on the *i–v* characteristics of the agglomerate, as shown in Fig. 6(b). This can be explained as follows: with an increase in partial pressure of water vapor, the amount of water content in the ionomer increases and thus, the ionomer conductivity also increases. This is expected to result in an increase in the current, since current is given by

$$I_{agg} = -\kappa_{agg} 4\pi r_{agg}^2 \frac{\partial \phi_{agg}}{\partial r}|_{r=r_{agg}} = -\kappa_{mem} 4\pi r_{agg}^2 \frac{\partial \phi_{mem}}{\partial r}|_{r=r_{agg}} \quad (22)$$

On the other hand, when the conductivity increases, the potential drop from the surface to the agglomerate–ionomer interface is less and thus, the potential gradient is decreased. These two opposing effects nullify each of their contributions and this results in producing no change in the agglomerate current. Use of the above equation for calculating agglomerate current does not mean that conductivity of membrane is the limiting factor. The current also depends on the potential gradient appearing in the equation. Since it is easy to relate the effect of partial pressure of water vapor on conductivity of membrane, the above equation was chosen to describe the effect of partial pressure of water vapor on agglomerate current. Moreover, if we use the equation based on oxygen reaction rate for current calculation:

$$I_{agg} = \int_0^{r_{agg}} 4\pi r^2 (n_e F R_{orr})\, dr = \int_0^{r_{agg}} 4\pi r^2 \left(a_a i_o \left\{ \frac{c_{O_2,agg}}{c^s_{O_2}} \exp\left(-\frac{\alpha n_e \eta_r F}{RT_{agg}}\right) - \exp\left(\frac{(1-\alpha) n_e \eta_r F}{RT_{agg}}\right) \right\} \right) dr \quad (23)$$

the effect of partial pressure of water vapor cannot be easily explained as it can be done using the earlier equation.

One of the limitations of this result is that, when carrying out the parametric studies, partial pressures of water vapor and oxygen are treated independently. But in actual fuel cell operation, this will not the case. This result will be further investigated in our research work on the dynamic model for PEM fuel cell cathode that is currently under progress. It is necessary to highlight at this juncture, that though all the four plots in Fig. 6(b) seem to merge, upon magnification it was observed that this was not the case. At a constant potential, the agglomerate currents differed from each other in third and fourth decimal points. This is also corroborated by the corresponding dynamic plots (see Fig. 16).

The model was also simulated for different agglomerate radii (r_{agg}). The *i–v* characteristic plots are shown in Fig. 7(a). At a constant surface potential, with increasing agglomerate radii, larger surface area is available for reaction. Hence, the

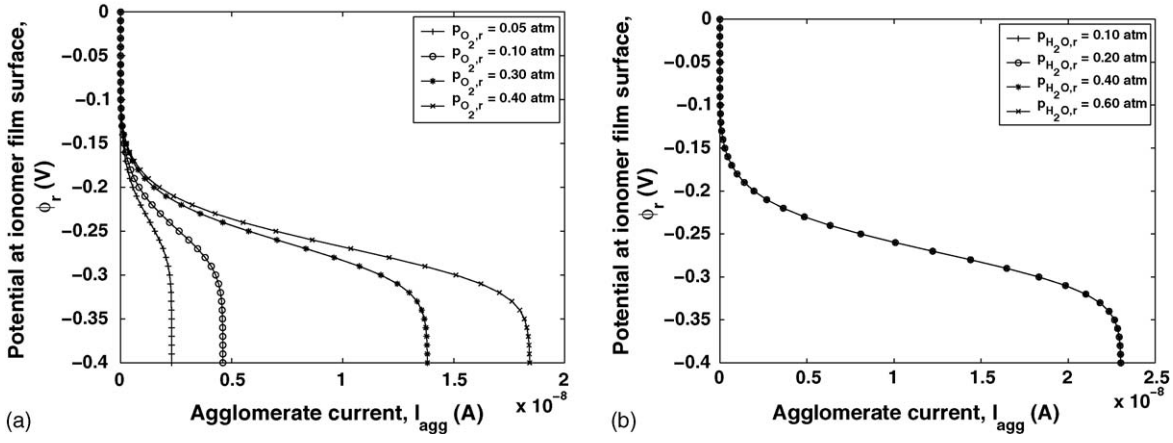

Fig. 6. Parametric studies of agglomerate characteristic curve: (a) variation in $p_{O_2,r}$ and (b) variation in $p_{H_2O,r}$.

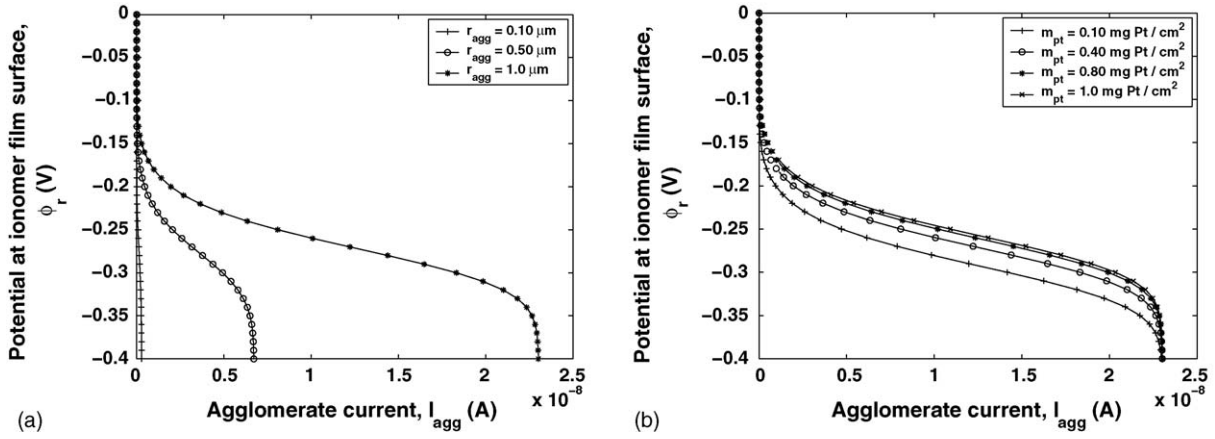

Fig. 7. Parametric studies of agglomerate characteristic curve: (a) variation in r_{agg} and (b) variation in m_{pt}.

agglomerate current increases. The effect of change in platinum loading (m_{pt}) on *i–v* characteristic plot is shown in Fig. 7(b). This figure shows some unique characteristics, different from Figs. 6(a) and 7(a). It can be observed that at a given potential (ϕ_r), agglomerate current increases with increasing platinum loading. This effect in the agglomerate is clearly seen for surface potentials in the range −0.15 to −0.35 V. At surface potentials between 0.0 and −0.15 V, the effect is not clearly observed from the plots due to the scale on the *x*-axis. But upon zooming on the plots between 0.0 and −0.15 V, the effect could be clearly seen. At surface potentials < −0.35 V, all the plots converge to the same limiting current value. This is due to the fact that the agglomerate current is limited by the total amount of dissolved oxygen and thus, platinum loading does not have any effect. This result suggests that there is an optimum loading for the platinum catalyst inside the PEMFC reaction layer.

The effect of different ionomer film thickness on the *i–v* curves is shown in Fig. 8(a). At a particular surface potential, with an increase in film thickness, the agglomerate current decreases. This is due to the fact that an ionomer film with higher thickness provides a higher resistance for diffusion of dissolved oxygen. This results in low concentrations of oxygen at the agglomerate–ionomer interface and hence, less amount of reaction leading to a decrease in current generated. On the other hand, at a constant surface potential, when the fraction of volume occupied by ionomer inside active agglomerate region (ϵ_{agg}) is increased, increase in agglomerate current is observed, Fig. 8(b). This is a result of the boundary condition, BC3, in Table 1. Presence of more ionomer in between the carbon agglomerates results in a higher supply of dissolved oxygen and thus, more reaction and more current. It should be noted that for this parameter study, catalyst loading (m_{pt}) and active catalyst area (a_{pt}) are kept constant at their base case values.

3.2. Dynamic model simulation

The agglomerate dynamic model was simulated for various conditions to gain insight into the dynamic characteristics of an agglomerate. The dynamic model is solved using ode15s, an ode solver in MATLAB. MATLAB's Simulink environment is used to simulate the dynamic model. Inputs to the model and model parameters are passed from the Simulink environment. Fig. 9 illustrates the set up of the dynamic model for spherical agglomerate in MATLAB's Simulink environment. The model is

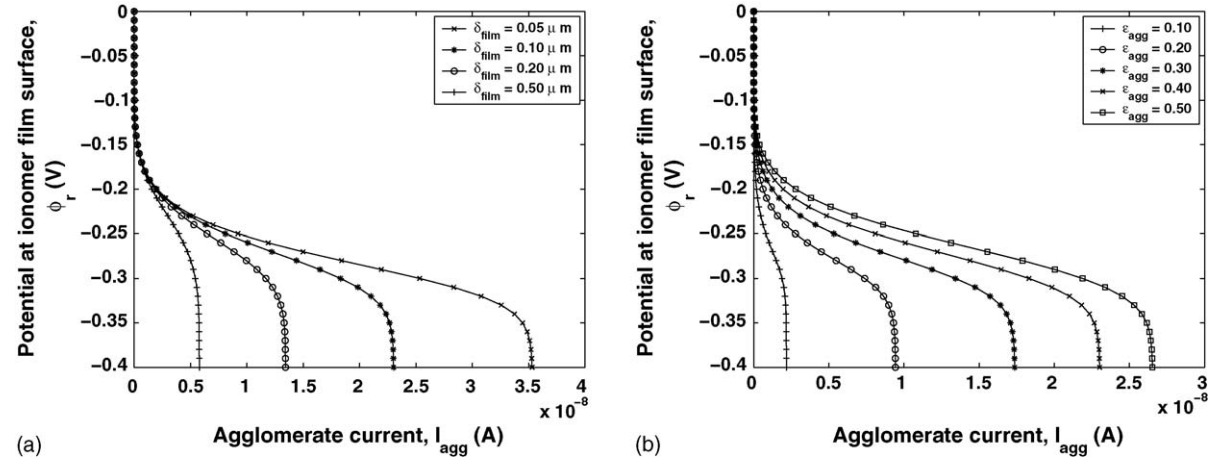

Fig. 8. Parametric studies of agglomerate characteristic curve: (a) variation in δ_{film} and (b) variation in ε_{agg}.

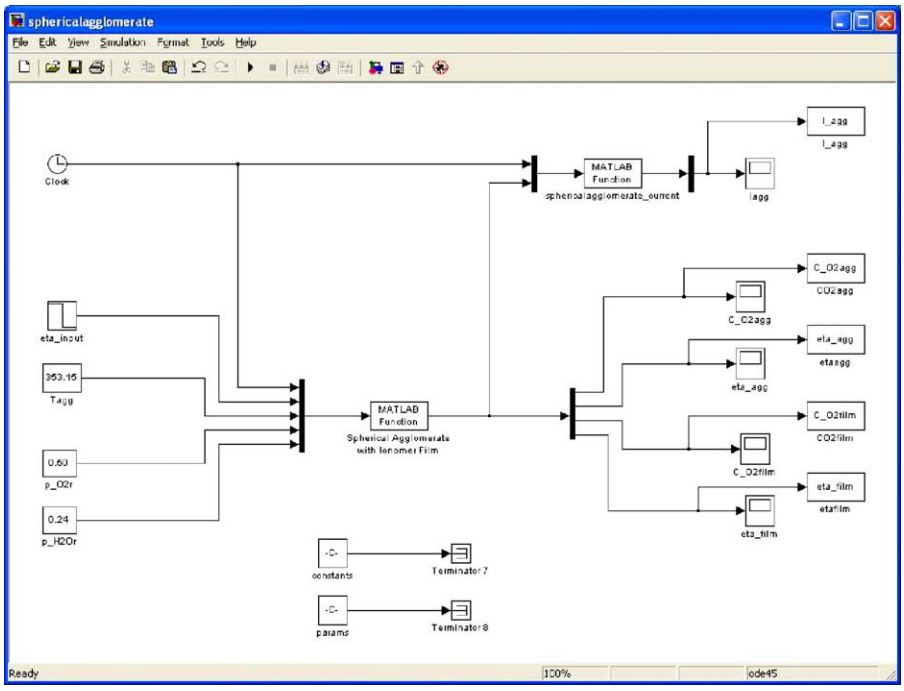

Fig. 9. Agglomerate dynamic model in Matlab's Simulink environment.

set up such that ionomer film surface potential (ϕ_r), partial pressures of oxygen ($p_{O_2,r}$) and water vapor ($p_{H_2O,r}$) at the surface of ionomer film and temperature of the agglomerate (T_{agg}) are taken as inputs. The dissolved concentration of oxygen ($c_{O_2,agg}$ and $c_{O_2,film}$), potential (ϕ_{agg} and ϕ_{film}), and the current generated from the agglomerate (I_{agg}) are the output variables. Initial conditions for simulation are provided by the corresponding steady-state model.

To determine the minimum time for which the dynamic simulation has to be run, the dynamic model equations are non-dimensionalised. Various time constants are identified and it was found that diffusive term of the potential equation (Eq. (19)) has the least time constant for the given set of parameters. The dynamic characteristics of an agglomerate are studied by introducing a step in surface potential and monitoring the transients in the output variables ($c_{O_2,agg}$, $c_{O_2,film}$, ϕ_{agg}, ϕ_{film}, and I_{agg}). Fig. 10 shows dynamic simulation results for variation in agglomerate potential (ϕ_{agg}) for a step in surface potential from -0.05 to -0.10 V. Different lines in the figure correspond to the different radial locations inside the spherical agglomerate. Even though the agglomerate is divided into 500 concentric spherical shells, profiles for only 11 radial locations, which includes $r = 0$ and $r = r_{agg}$, are illustrated in the figures for clarity. Fig. 10(a) shows simulation results for time between $t = 0$ and 1.4×10^{-6} s. It can be clearly seen that agglomerate potential reaches steady-state well within the simulation time. On the other hand, when the model is simulated from $t = 0$ to 0.035 s (Fig. 10(b)), no transients are observed for all the radial locations. All the 11 lines plotted in the figure coincide and an instantaneous step response is observed.

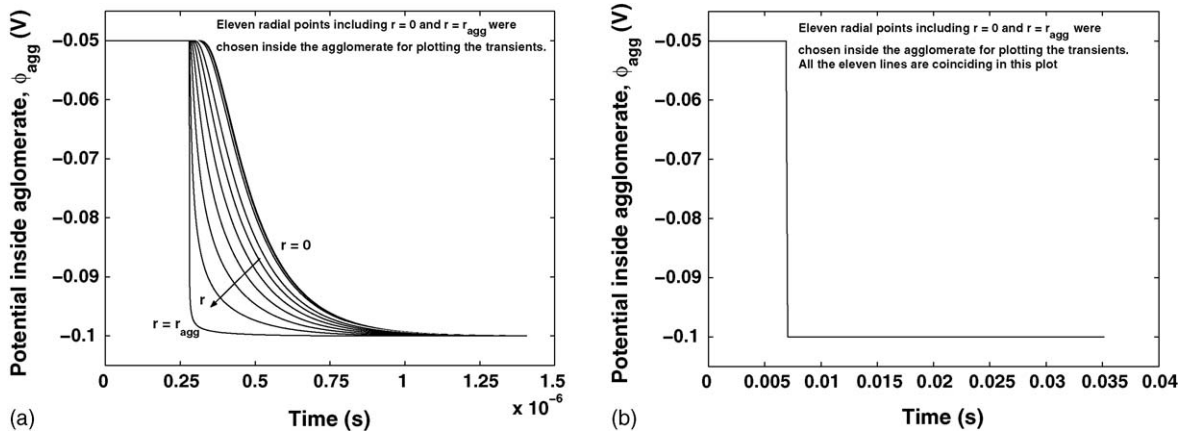

Fig. 10. Dynamic simulation for agglomerate potential, ϕ_{agg}: (a) simulation from time $t = 0$ to 1.4×10^{-6} s and (b) simulation from $t = 0$ to 0.035 s.

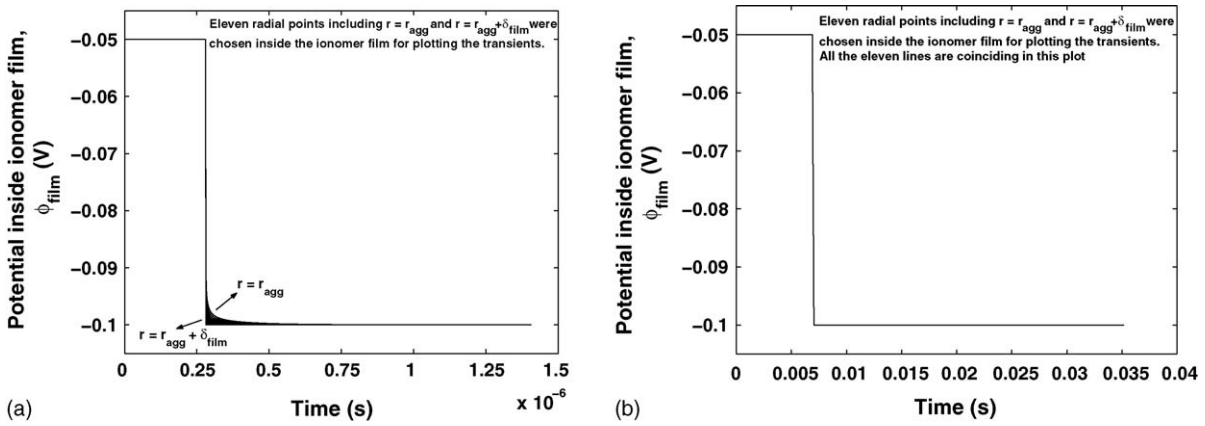

Fig. 11. Dynamic simulation for potential inside ionomer film, ϕ_{film}: (a) simulation from time $t = 0$ to 1.4×10^{-6} s and (b) simulation from $t = 0$ to 0.035 s.

The corresponding dynamic simulation results for potential inside the ionomer film (ϕ_{film}) are shown in Fig. 11. Even though while writing the dynamic model, no charge accumulation was considered inside the ionomer film, it still exhibits a small amount of transients when the model is simulated for the time between $t = 0$ and 1.4×10^{-6} s (Fig. 11(a)). These transients arise due to the boundary conditions at the agglomerate–ionomer interface. Similar to the dynamic behavior of ϕ_{agg}, when the model is simulated from $t = 0$ to 0.035 s (Fig. 11(b)), no transients are observed.

The corresponding dynamic simulation results for dissolved concentration of oxygen inside agglomerate and ionomer film are shown in Figs. 12 and 13, respectively. The concentrations are plotted in normalized scale. The model is run under steady conditions from $t = 0$ to 0.01 s and then a step in surface potential from −0.05 to −0.10 V is introduced. Fig. 12(a) shows the simulation results for time between $t = 0$ and 1.4×10^{-6} s. A flat profile is observed at all radial locations for the complete time interval. This can be explained by the fact that the time interval being very small, the concentrations at all radial locations do not show any change from their steady-state profile corresponding to the surface potential of −0.05 V. The transients in oxygen concentration are observed only when the model is simulated from $t = 0$ to 0.035 s, as illustrated in Fig. 12(b). The transients exhibited by the dissolved concentration of oxygen inside the ionomer film (Fig. 13) are similar to that of the concentration inside the agglomerate. It should be noted that the range of y-axis in Figs. 12 and 13 is very small. This is due to the magnitude of the potential chosen for the step response (−0.05 to −0.10 V). Dynamic simulations for a step in potential from −0.25 to −0.30 V were also performed using the model. The qualitative behavior of the transients exhibited by the potential and concentration inside agglomerate and ionomer film was found to be same. But the variation of normalised concentration of dissolved oxygen was found to be significant.

The time response of agglomerate current (I_{agg}) for step in surface potential from −0.05 to −0.10 V is shown in Fig. 14(a). It can be observed that agglomerate current shows an instantaneous jump and then decreases to a steady value. That is, it shows an inverse response. We abuse standard terminology a little bit in terming this phenomenon as inverse response. In standard control literature, inverse response is a phenomenon where the initial derivative sign is different from the sign of the final steady-state gain. However, the phenomenon we observe is a sudden jump and a subsequent drop in the value, albeit with the same sign for the initial derivative and the final steady-state

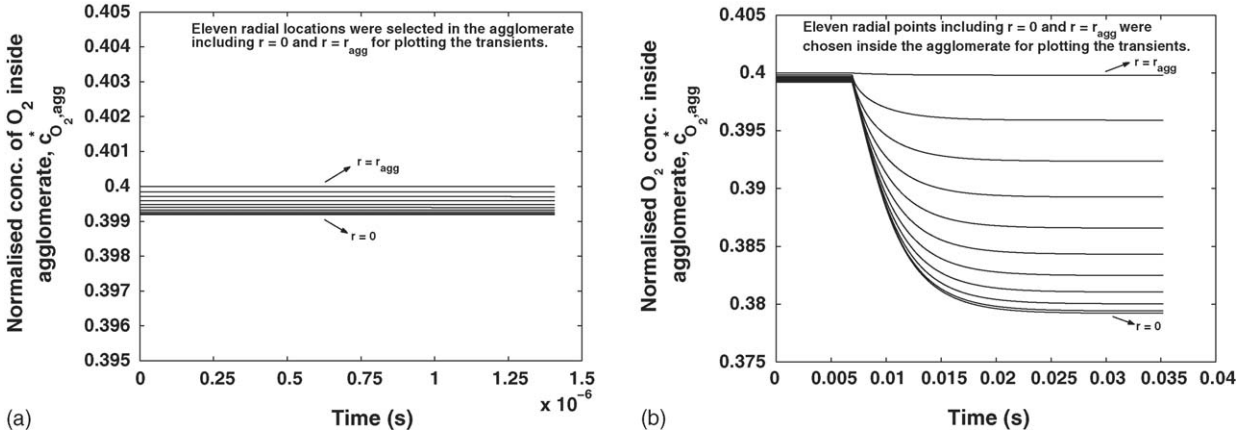

Fig. 12. Dynamic simulation for normalized concentration of dissolved O_2 inside agglomerate, $c^*_{O_2,\text{agg}}$: (a) simulation from time $t = 0$ to 1.4×10^{-6} s and (b) simulation from $t = 0$ to 0.035 s.

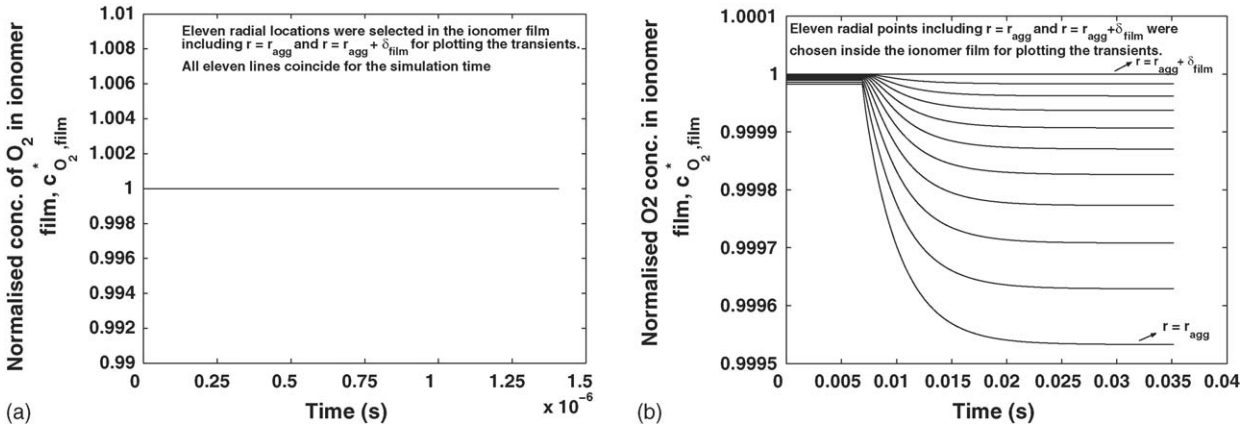

Fig. 13. Dynamic simulation for normalized concentration of dissolved O_2 inside ionomer film, $c^*_{O_2,film}$: (a) simulation from time $t = 0$ to 1.4×10^{-6} s and (b) simulation from $t = 0$ to 0.035 s.

gain. This can be explained by observing the plots in Figs. 10(b) and 12(b). When a step is introduced in the surface potential, the agglomerate potential (ϕ_{agg}) shows an instantaneous response, see Fig. 10(b). However, the dissolved concentration of oxygen does not show instantaneous response. Hence, a higher agglomerate potential and high concentration of dissolved oxygen are the reason for instantaneous jump in the agglomerate current. Subsequently, the dissolved concentration of oxygen decreases to the new steady-state values corresponding to $\phi_r = -0.10$ V, see Fig. 12(b). This reduced concentration and time delay causes the agglomerate current to settle down to its new steady-state value. In Fig. 14(a), the magnitude of the inverse response is small due to the magnitude of the surface potential. A similar inverse response in agglomerate current is observed for step in surface potential from −0.25 to −0.30 V, Fig. 14(b). The effect of potential magnitude on the magnitude of inverse response can be clearly seen in this plot. In order to check whether the simulation results are correct, the steady-state values of the agglomerate current in Fig. 14 are compared with those predicted in the *i–v* curves, Fig. 5. The values are found to be same.

The dynamics of agglomerate current in response to a step in partial pressure of oxygen at the surface are illustrated in Fig. 15. The dynamics are studied at two different surface potentials, −0.15 and −0.30 V. For both cases, simulation results show that the agglomerate current increases to a new steady-state value with some dynamics. In addition, the plots show that at higher potential, the dynamics of the agglomerate current is faster, i.e., it reaches steady-state in lesser time.

The dynamic results corresponding to step in partial pressure of water vapor at the surface ($p_{H_2O,r}$) are given in Fig. 16. When the surface partial pressure of water vapor is increased, agglomerate current decreases to a new steady-state value showing inverse response. This inverse response can be explained using the reason provided for the steady-state result in Fig. 6(b). When a step is introduced in the partial pressure of water vapor at the surface, the water content of the ionomer increases. This in turn, results in a higher ionomer conductivity (κ_{mem}). Due to high conductivity, the potential drop from the ionomer surface to the agglomerate–ionomer interface decreases. This change in potential is instantaneous, which is exhibited as a sudden drop in the current, see Fig. 16(a) and (b). However, the dissolved concentration of oxygen increases slightly to a new steady value, but with a time delay. This causes the agglomerate current

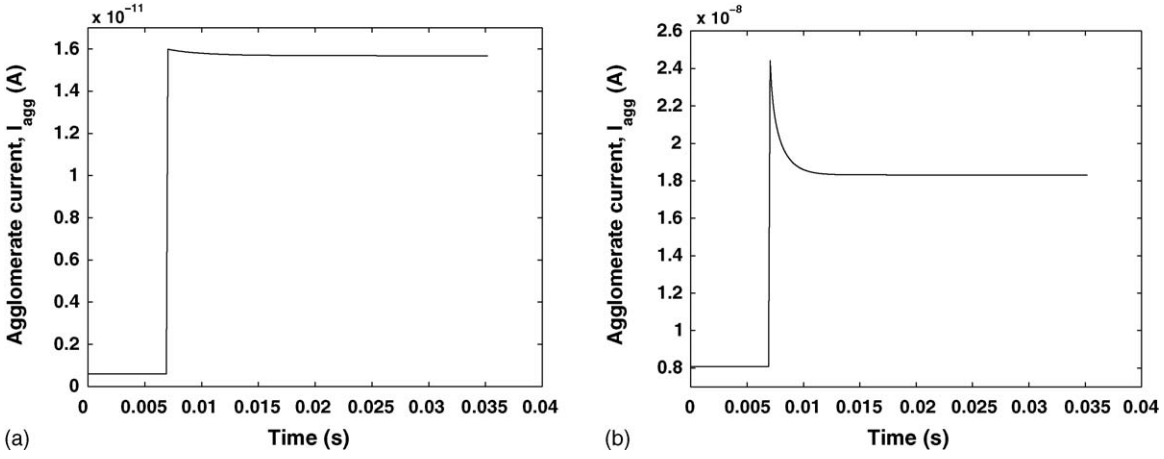

Fig. 14. Transients in agglomerate current, I_{agg}, for step in ϕ_r: (a) step in ϕ_r: −0.05 to −0.10 V and (b) step in ϕ_r: −0.25 to −0.30 V.

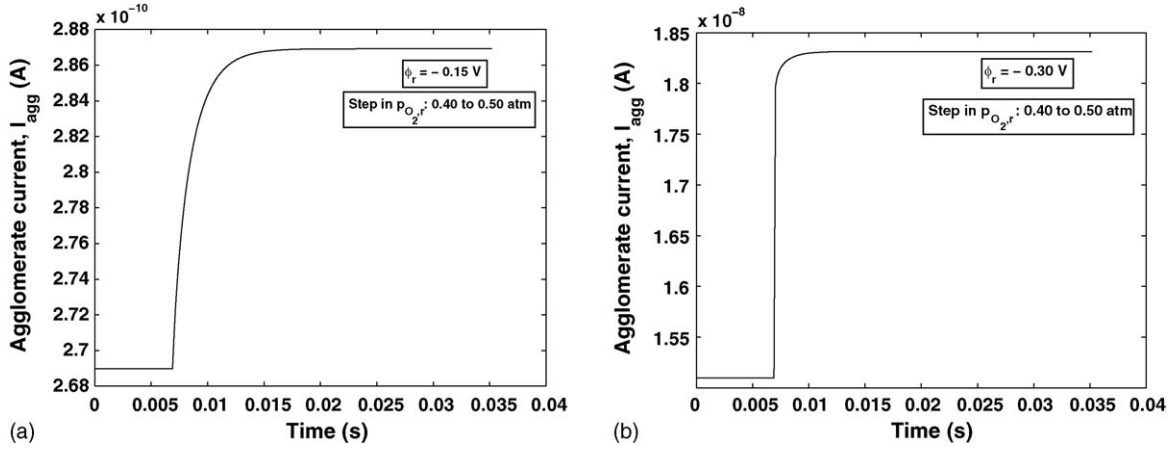

Fig. 15. Transients in agglomerate current, I_{agg}, for step in $p_{O_2,r}$: (a) step in $p_{O_2,r}$: 0.30–0.40 atm and (b) step in $p_{O_2,r}$: 0.30–0.40 atm

to increase to its new steady-state value with the same time delay.

From the y-axis in Fig. 16(a) and (b), it can be observed that the variation in current is small. This corroborates the plot shown in Fig. 6(b), which shows that the partial pressure of water vapor has negligible effect on agglomerate current.

The transients shown for agglomerate current (I_{agg}) for step changes in surface potential are typical and are also observed in dynamic response of fuel cells. This kind of behavior is also shown by Wang and Wang [25]. They have shown the dynamic response of average cell current density to the step changes of cell voltages. The plots show surge in the current densities that occur in time scales that are of the same order of magnitude as shown in Fig. 14. Our ultimate goal is to use these dynamic models to study operational problems in PEM fuel cells and stacks. Significant work has been done earlier in our research group for phosphoric acid fuel cells (PAFC) using the dynamic models of spherical agglomerates. It was shown that these models can be used for identification of problems during the operation of large sized PAFC cells [26,27].

All the simulation results presented above using steady-state and dynamic model of spherical agglomerate can be extrapolated to understand the behavior of PEM fuel cell cathode. Since it was convenient to carry out the numerical simulations, oxygen electrode was assumed as the reference electrode. The same studies can also be done considering that the potential of the solid phase inside the agglomerate is measured against a standard hydrogen electrode (SHE). In such a case, the local overpotential inside the agglomerate (η_r) is defined as

$$\eta_r = V_{agg} - V_{agg,e} - \phi_{agg} \tag{24}$$

where V_{agg} is the potential of the solid phase inside the agglomerate measured against SHE. The subscript e denotes equilibrium conditions. The i–v characteristic curve and other trends shown in the plots for parametric studies will not change if simulations were carried out using Eq. (24) instead of Eq. (13b). Moreover, all the trends that are shown in the plots for dynamic studies will also remain the same. Hence, all the above results can be extrapolated and used as a basis to understand the steady-state and dynamic behavior of fuel cell cathode.

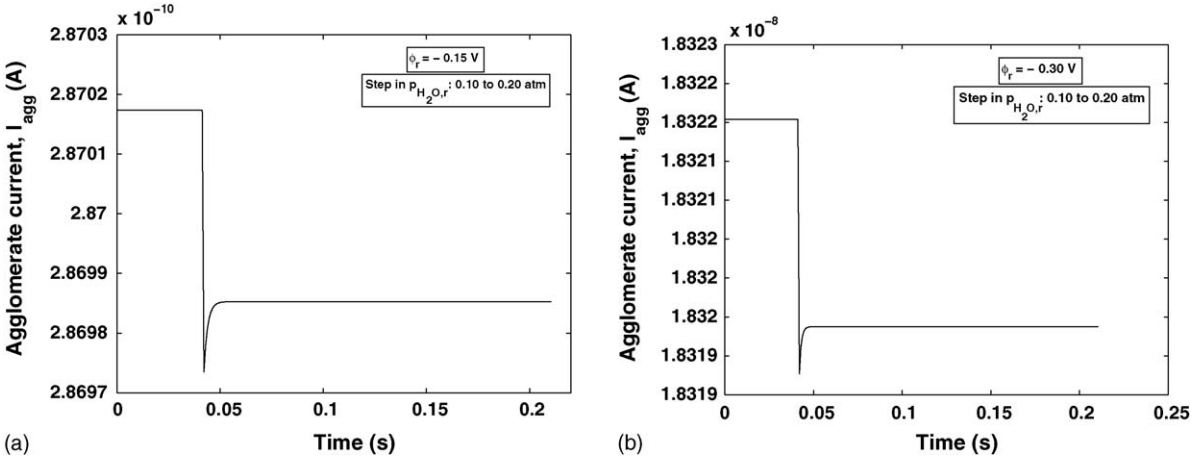

Fig. 16. Transients in agglomerate current, I_{agg}, for a step in $p_{H_2O,r}$: (a) step in $p_{H_2O,r}$: 0.10–0.20 atm and (b) step in $p_{H_2O,r}$: 0.10–0.20 atm.

4. Conclusions

A dynamic model for spherical flooded-agglomerate has been described in this work. The flooded-agglomerate consists of a thin film of ionomer covering a uniform mixture of carbon supported platinum and ionomer. The model takes into consideration the conservation of dissolved oxygen and hydrogen ions. The complete characteristic curve of the agglomerate is predicted by the model. The influence of surface boundary conditions and model parameters on the i-v curve were presented. In addition, dynamics of agglomerate potential, dissolved concentration of oxygen and agglomerate current for step input in surface boundary conditions were also presented.

In summary, the significant findings of this work are:

- potential variation inside the flooded agglomerate and ionomer film is important as significant gradients exist inside the agglomerate and ionomer film,
- with the help of dynamic model studies, it was shown that the time required to reach steady state for dynamics of dissolved oxygen concentration and potential differ by several orders of magnitude (10^{-2} and 10^{-6} s, respectively). The difference in time scale in the transients of potential and concentration seems to suggest that the dynamics of agglomerate potential can be neglected and the overall dynamics of the agglomerate model is governed by the dynamics of dissolved concentration of oxygen, $c_{O_2,agg}$ and $c_{O_2,film}$
- the dynamic response of agglomerate current (I_{agg}) to step changes in surface boundary conditions have been highlighted. The time required to reach steady state for the agglomerate current is strongly influenced by the potential at the ionomer film surface.

All the above results and effects have been studied and described at a single agglomerate level. And moreover, the influence of boundary conditions and parametric studies have been done one at a time, i.e., without considering the effect of one boundary condition on another and one model parameter on another. In the case of complete PEM fuel cell, this would not be the scenario. There would be averaging effects of agglomerates within the reaction layer, influence of gas phase transport and liquid water, and boundary conditions that cannot be treated independently. These effects are currently being investigated by our group as a part of the work on dynamic model for PEM fuel cell cathode.

Acknowledgements

We would like to acknowledge American Chemical Society – Petroleum Research Fund (ACS-PRF) for providing financial support for this work. Grant # PRF 42842-AC9.

References

[1] T.E. Springer, T.A. Zawodzinski, S. Gottesfeld, J. Electrochem. Soc. 138 (1991) 2334–2342.
[2] D.M. Bernardi, M.W. Verbrugge, AIChE J. 37 (1991) 1151–1163.
[3] D.M. Bernardi, M.W. Verbrugge, J. Electrochem. Soc. 139 (1992) 2477–2491.
[4] A.J. Appleby, F.R. Foulkes, Fuel Cell Handbook, Van Nostrand Reinhold, New York, 1989.
[5] M.B. Cutlip, S.C. Yang, P. Stonehart, Electrochim. Acta 36 (1991) 547–553.
[6] A.D. Tantram, A.C.C. Tseung, Nature 221 (1969) 167–168.
[7] J. Giner, C. Hunter, J. Electrochem. Soc. 116 (1969) 1124–1130.
[8] S.C. Yang, M.B. Cutlip, P. Stonehart, Electrochim. Acta 35 (1990) 869–878.
[9] H. Celiker, M.A. Al-saleh, S. Gultekin, A.S. Al-zakri, J. Electrochem. Soc. 138 (1991) 1671–1681.
[10] M.A. Al-Saleh, S. Gultekin, S.U. Rahman, A. Al-Zakri, J. Power Sources 55 (1995) 33–39.
[11] M.L. Perry, J. Newman, E.J. Cairns, J. Electrochem. Soc. 145 (1998) 5.
[12] G. Maggio, J. Appl. Electrochem. 29 (1999) 171–176.
[13] S.R. Choudhury, M.B. Deshmukh, R. Rengaswamy, J. Power Sources 112 (2002) 137–152.
[14] N.P. Siegel, M.W. Ellis, D.J. Nelson, M.R. von Spakovsky, J. Power Sources 115 (2003) 81–89.
[15] G. Lin, W. He, T.V. Nguyen, J. Electrochem. Soc. 151 (2004) A1999–A2006.
[16] Q. Wang, D. Song, T. Navessin, S. Holdcroft, Z. Liu, Electrochim. Acta 50 (2004) 725–730.
[17] D. Song, Q. Wang, Z. Liu, T. Navessin, S. Holdcroft, Electrochim. Acta 50 (2004) 731–737.
[18] Q. Wang, M. Eikerling, D. Song, Z. Liu, J. Electroanal. Chem. 573 (2004) 61–69.
[19] E. Middleman, Fuel Cells Bull. (2002) 9–12.
[20] S.J. Lee, S. Mukerjee, J. McBreen, Y.W. Rho, Y.T. Kho, T.H. Lee, Electrochim. Acta 43 (1998) 3693–3701.
[21] F. Liu, B. Yi, D. Xing, J. Yu, Z. Hou, Y. Fu, J. Power Sources 124 (2003) 81–89.
[22] Q. Guo, M. Cayetano, Y. Tsou, E.S.D. Castro, R.E. White, J. Electrochem. Soc. 150 (2003) A1440–A1449.
[23] C. Wang, A.J. Appleby, J. Electrochem. Soc. 150 (2003) A493–A498.
[24] Z. Ogumi, Z. Takehara, S. Yoshizawa, J. Electrochem. Soc. 131 (1984) 769–773.
[25] Y. Wang, C.Y. Wang, Electrochim. Acta 50 (2005) 1307–1315.
[26] S.R. Choudhury, PhD Thesis, Indian Institute of Technology, Bombay, India, 2004.
[27] S.R. Choudhury, R. Rengaswamy, (2005), submitted for publication.